

A new viewpoint and model of neural signal generation and transmission: Signal transmission on myelinated neuron*

Zuoxian Xiang(向左鲜)^{1,2}, Chuanxiang Tang(唐传祥)¹, Lixin Yan(颜立新)¹,
Chao Chang(常超)^{2,†}, and Guozhi Liu(刘国治)^{1,‡}

¹Department of Engineering Physics, Tsinghua University, Beijing 100084, China

²Innovation Laboratory of Terahertz Biophysics, National Innovation Institute of Defense Technology, Beijing 100071, China

(Received 9 January 2020; revised manuscript received 28 July 2020; accepted manuscript online 13 August 2020)

Based on our previous work, we study the problem of neural signal transmission of myelinated neurons. We found that the transmembrane ion current at Ranvier's node acts as an energy supplement. In addition, the length of the myelin sheath has an upper limit of l_T . Above this upper limit, the neural signal will not be effectively transmitted. In the range of normal physiological parameters, l_T is on the order of mm. Finally, the effect of temperature on the transmission of nerve signals is investigated. temperatures that are too high and too low are not conducive to the conduction of nerve signals.

Keywords: THz, myelinated neuron, signal transmission

PACS: 87.10.Vg, 87.10.Ca, 87.85.Ng

DOI: [10.1088/1674-1056/abace9](https://doi.org/10.1088/1674-1056/abace9)

1. Introduction

Neural signal generation and transmission are the most fundamental and important issue in neuroscience. Researchers have established a series of models to study the transmission of neural signals and the most widely used models (such as the Hodgkin-Huxley's model) are based on the assumption of a neuron equivalent circuit.^[1–10] While, we thought that the neural information transmission model based on equivalent circuits could not explain the following questions. Firstly, the time scale of the signal obtained by the model is on the order of ms, the corresponding frequency is in the kHz range, as the information carried by the kHz signal is very small and the transmission speed is very low (~ 20 m/s), complex physiological activities (such as learning and memory, logical reasoning, *etc.*) need to process a large amount of information, how does the signal of the kHz level meet the needs of the nervous system for a large amount of information transmission and processing? Secondly, the skin depth of the kHz range electromagnetic field is on the order of meters and is much larger than the neurological scale, and the signals of different neurons will interfere with each other, the higher the frequency, the smaller skin depth. When the electromagnetic field frequency exceeds the THz level, it can effectively avoid interference between different neurons. In addition, other scholars have also proposed neural information-related models from different perspectives, such as GHz^[11,12]/infrared^[13–15] electromagnetic field information model, neuron-microtubule-based quantum information model,^[16–19] quantum confinement su-

perfluid model,^[20] *etc.*

We build a neural signal generation and transmission model from a new perspective. Traditional circuit models describe neural signals with voltage. Voltage signals are the integral form of electric field signals. Compared with voltage signals, electromagnetic fields are more basic physical quantities. The physical model will use electromagnetic fields to describe neural signals. We thought that the frequency of nerve signals should be in the order of THz, and the action potential does not represent the essence of neural information. In addition to the reasons described above, there are the following reasons: (i) The process of nerve signal transmission is accompanied by the movement of ions. The movement of ions is inseparable from ion-ion interaction, ion-ion channel interaction, ion-water molecule interaction, the frequency of the characteristic energy of these interactions is in the order of THz to mid-infrared, THz electromagnetic fields are easily coupled with these processes, allowing the THz signals to be effectively transmitted. (ii) The nerve signal is greatly affected by temperature, while the heat radiation at normal body temperature. The characteristic energy is also in the order of THz to mid-infrared.

In our previous papers,^[21–23] we proposed several conjectures about the generation and transmission of neural signals and discussed the eigenmodes and dispersion relationships of high-frequency neural signals and signal transmission problems on unmyelinated nerve fibres. The main results are: i) neural signals include low-frequency action potentials and high-frequency electromagnetic fields (whose frequencies

*Project supported in part by the National Defense Technology Innovation Special Zone and the National Natural Science Foundation of China (Grant Nos. 51677145 and 11622542).

†Corresponding author. E-mail: changc@xjtu.edu.cn

‡Corresponding author. E-mail: liuguozhi60@163.com

are in THz and infrared bands); ii) the envelope of high-frequency signals is slowly changing, and high-frequency signals and low-frequency action potentials signals travel at the same speed.

Based on our previous research, we study the signal transmission in myelinated neurons. In this paper, we mainly study two issues: (I) Take action potential signal as an example, study the influence of myelin length on signal transmission and the role of Ranvier's nodes, and explain our point of view: Ranvier's nodes play the role of energy supply; (II) Predict the influence of temperature on nerve signal transmission (including high-frequency and low-frequency signals), and design related experiments to verify the effect of temperature on nerve conduction velocity. The influence of temperature on other processes still needs experimental verification.

2. Modelling

Firstly, we introduce the modelling ideas briefly. The neural signals in the model are described by the electromagnetic fields. The electromagnetic field transmission process is mainly affected by three factors: I) the distribution of the medium in the geometric space, II) the electromagnetic parameters of the medium (dielectric constant, conductivity, the coupling coefficient of electromagnetic field-molecular interaction, *etc.*) III) the source of electromagnetic field. In view of the above three factors, in our model, the following approximations are made: The first is that the model only considers the transmission of nerve signals along the axon, the axon surface is equivalent to an ideal cylindrical surface. Note that the x axis is the direction of nerve signal propagation (parallel to the surface of the neuron axon). The second one is the main components of neuronal cell fluid are water molecules, ions, and other neutral molecules. The content of other neutral molecules is very small, and their effects are not considered in the model, and the model mainly considers the electromagnetic parameters of water molecules and ions. Due to the effect of the electrostatic field on the surface of the cell membrane of the neuron, the water molecules near the surface of the cell membrane could form a long-range ordered structure, which makes the refractive index of the electromagnetic field higher at certain characteristic frequencies and reduces the loss of the THz signal.^[22] The electromagnetic field is mainly confined in the limited area of the neuron surface (including the myelin sheath). The third one is the source of the electromagnetic field in the model is generated by the movement of ions across the membrane.

In our previous work,^[21–23] we used quantum mechanics, electrodynamics, and other theories to study the transmission of electromagnetic field signals in nerves and established a dy-

namic equation for neural signal transmission:

$$\begin{cases} i \frac{\partial \psi_n}{\partial t} = \varepsilon_n \psi_n - \sum_{\lambda, m} \eta_{n, m, \lambda} A_\lambda \psi_m, \\ \frac{\partial^2 A_\lambda}{\partial t^2} + \gamma \frac{\partial A_\lambda}{\partial t} + \omega_p^2 A_\lambda - c_\lambda^2 \nabla^2 A_\lambda \\ - \sum_{m, n} \eta_{m, n, \lambda} \psi_n^+ \psi_m = J_\lambda(\mathbf{r}, t), \end{cases} \quad (1)$$

where $|\psi_n|^2$ is the number of water molecules at energy level n per unit volume, ε_n is the energy value corresponding to different energy levels of water molecules, $\eta_{n, m, \lambda}$ is the coupling coefficient of water molecule–electromagnetic field interaction, A_λ ($\lambda = 1, 2, 3$) is the three components of the electromagnetic field vector potential function, the space electromagnetic field is determined by $\mathbf{E} = -\partial \mathbf{A} / \partial t$, $\mathbf{B} = \nabla \times \mathbf{A}$, γ is the energy loss constant of the electromagnetic field, ω_p is the ion oscillation frequency,

$$c_\lambda = \begin{cases} c & (\lambda = 1, 2), \\ \beta & (\lambda = 3), \end{cases}$$

where c is the speed of light in the medium (the value is smaller than the speed of light in vacuum), β is the speed of ion sound, its value is in the order of 1000 m/s,^[24] $J_\lambda(\mathbf{r}, t)$ is the ion transport current across the membrane. The natural unit $\hbar = c = 1$ was used.

The eigenmode of the system is discussed in Ref. [21]. The parameter ε_n , ω_p in Eq. (1) is in the THz range, and the intrinsic mode of the electromagnetic field transmission of the system is also in the THz range. By considering the contribution of ion transmembrane transport current, we will describe the characteristics of the neural signal predicted according to Eq. (1) in the following.

$J_\lambda(\mathbf{r}, t)$ is the current transported by ions across the membrane. The numerical simulation results^[23] shows that in short time scale (from ps to ns scale) and a space scale in a single ion channel (\sim nm), the ion transport current oscillates rapidly, and its oscillation frequency is in the order of THz. However, for the statistical results of a long time scale (\sim ms) and a large number of ion channels, the ion transport current across the membrane has a low-frequency component, namely,

$$J(x, t) = \langle J(x, t) \rangle + \tilde{J}(x, t), \quad (2)$$

where $\langle J(x, t) \rangle$ is a low-frequency ion current (\sim kHz); and $\tilde{J}(x, t)$ is a high-frequency component in the ion transport process. $\tilde{J}(x, t)$ is caused by ion–ion channel interaction.

Since $J(x, t)$ has two different time scales, electromagnetic fields for different time scales will be excited, that is to say, the electromagnetic field in space has the following form:

$$E(x, t) = \langle E(x, t) \rangle + \tilde{E}(x, t). \quad (3)$$

Here, $\langle E(x, t) \rangle$ is the low-frequency electromagnetic field caused by $\langle J(x, t) \rangle$ that changes slowly with time, and $\tilde{E}(x, t)$ is

the high-frequency electromagnetic field of the system. $\tilde{E}(x, t)$ excited by the coupling between high-frequency current transported by ions across the membrane and the high-frequency intrinsic mode of the neuron.

The calculation of electromagnetic field transmission of myelinated nerves is discussed below. Figure 1 shows the structural features of myelinated nerve fibres. Microscopically, in contrast to unmyelinated neurons, the ion channels of myelinated neurons are mainly distributed near the Ranvier's node, and there are very few ion channels in the area far from the Ranvier's node.^[25,26] Since the ion transmembrane transport process mainly relies on the contribution of ion channels, as a preliminary approximation. The ion transmembrane transport current J_m is not 0 near the Ranvier's node, and no transmembrane ion transport current is located elsewhere, namely,

$$J_m(x, t) \begin{cases} \neq 0, & x_l - \Delta x < x < x_l + \Delta x, \\ = 0, & \text{else,} \end{cases} \quad (4)$$

where $x_l - \Delta x < x < x_l + \Delta x$ is the area where there is an ion channel near the l -th Ranvier's node, Δx is generally in the order of 10 to several tens of μm . x_l is the coordinate of the center position of the l -th Ranvier's node. L_0 is used to indicate the length of Ranvier's node. L_0 is generally around 2 μm . $L = x_{l+1} - x_l - L_0 \approx x_{l+1} - x_l$ is the length of the myelin sheath (The length of the myelin sheath is about 100 times the diameter of the nerve^[8] and the diameter of myelinated nerve is generally several microns to tens of microns).

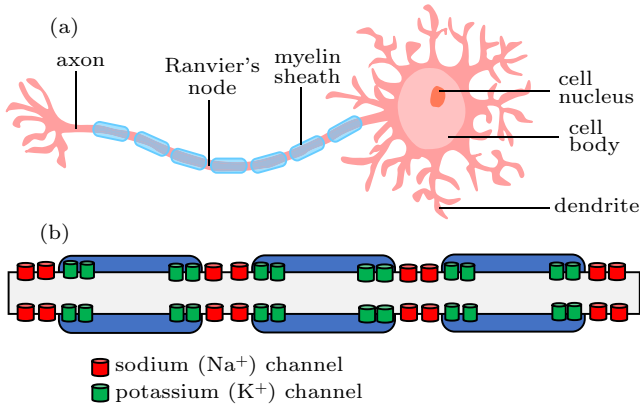


Fig. 1. (a) Schematic diagram of a myelinated nerve fibre structure and (b) schematic diagram of the myelinated nerve fibre ion channel distribution.

Equation (3) shows that the two kinds of electromagnetic field signals with different time scales in the nerve. On a long time scale, the equation is averaged and the electric field is described by the membrane potential $U(x, t)$ (the membrane potential divided by the thickness of the membrane is the electric field). It can be mathematically proved that the membrane potential $U(x, t)$ satisfies the differential equation $C\dot{U} = \sigma\partial^2 U/\partial x^2 + \langle J(x, t) \rangle$, which is consistent with the usual neural Cable model. For the electromagnetic field in the short time scale, under the approximation of two energy levels,

equation (1) changes into

$$\begin{cases} i\dot{\psi}_0 = \varepsilon_0\psi_0 - \sum_{\lambda} \eta_{\lambda} A_{\lambda} \psi_1, \\ i\dot{\psi}_1 = \varepsilon_1\psi_1 - \sum_{\lambda} \eta_{\lambda} A_{\lambda} \psi_0, \\ \frac{\partial^2 A_{\lambda}}{\partial t^2} + \gamma \frac{\partial A_{\lambda}}{\partial t} + \omega_p^2 A_{\lambda} - c_{\lambda}^2 \nabla^2 A_{\lambda} \\ = \eta_{\lambda} (\psi_0^+ \psi_1 + \psi_0 \psi_1^+) + \tilde{J}_{m,\lambda}(r, t). \end{cases} \quad (5)$$

Under the perturbation approximation, the THz electromagnetic field satisfies Eq. (6) in the frequency domain^[22]

$$-\omega^2 \Delta A_{\lambda} + (\omega_p^2 + c_{\lambda}^2 k^2 + i\gamma\omega) \Delta A_{\lambda} - \frac{2\omega_0^2 \omega_p^2}{g(g^2 \omega_0^2 - \omega^2)} \delta_{\lambda} \sum_{\mu} \delta_{\mu} \Delta A_{\mu} = \tilde{J}_m(k, \omega), \quad (6)$$

where $\delta_{\lambda} = \sqrt{n/\omega_0}(\eta_{\lambda}/\omega_p)$ is the normalized coupling coefficient, ω_0 is the transition frequency between two energy levels of water molecules, n is the number of water molecules per unit volume. For the myelinated nerves, the ion channels are mainly distributed near Ranvier's node and the transmembrane ion current is almost zero at the myelin (Eq. (1)), it will lead to differences between the myelinated and unmyelinated when the signal propagate along neuron axons, and the transmission characteristics of myelinated nerve will be discussed below.

The value of each parameter and the detailed method for the calculation of high-frequency and low-frequency signals was shown in the [Supplementary file](#).

3. Main results

Based on the methods presented in the [Supplementary file](#), in this section, we mainly study the two issues:

Issue 1 Take action potential signal as an example, we study the influence of myelin length on signal transmission and the role of Ranvier's nodes, and explain our point of view: Ranvier's nodes play the role of energy supply;

Issue 2 As a theoretical model, we hope to predict some experimental results as much as possible in order to compare with future experimental research, and we predict the influence of temperature on nerve signal transmission (including high-frequency and low-frequency signals), and design related experiments to verify the effect of temperature on nerve conduction velocity. The influence of temperature on other processes still needs experimental verification.

At first, we briefly introduce the characteristics of signals at different time scales. As shown in Fig. 2, the numbers of Ranvier's node on the neurons are noted by $j = 0, 1, \dots, N$. Stimulation was applied at $j = 0$ and $t = 0$ ms. Note that A and C are the center position of the j -th and $(j + 1)$ -th Ranvier's nodes, the midpoint of A and C is B .

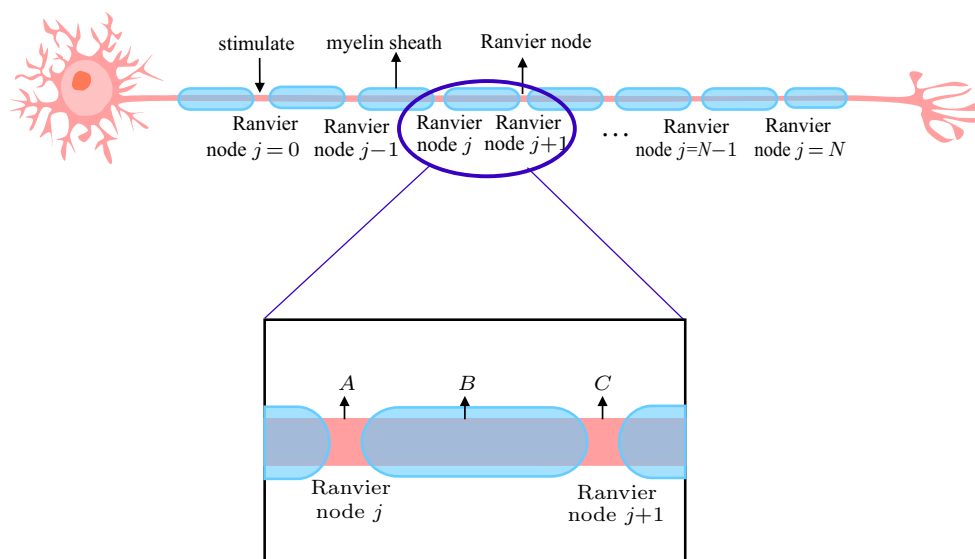


Fig. 2. Schematic diagram of the model.

Figure 3 shows the action potential waveform at $j = 10$, $j = 20$, and $j = 30$ Ranvier's nodes, where we take the neuron diameter as $10 \mu\text{m}$, the myelin sheath length as 1mm , and the ambient temperature as $20 \text{ }^\circ\text{C}$. It can be seen from the figure that the time scale of the low-frequency action potentials is in the order of ms, and the voltage amplitude is in the order of tens of mV. On the ms time scale, the time-domain waveforms of the action potentials at each Ranvier's node are almost the same, which can be calculated that the conduction velocity is about 14.3 m/s . For the same neuron diameter, the conduction velocity of myelinated nerves is much faster than that of unmyelinated nerves.

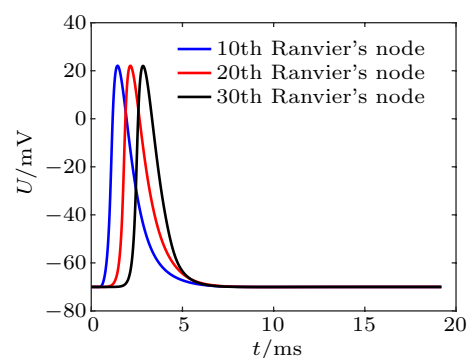


Fig. 3. Time-domain waveforms of low-frequency action potentials at different Ranvier's nodes (The action potential at $j = 10$, $j = 20$, and $j = 30$ Ranvier's nodes were shown).

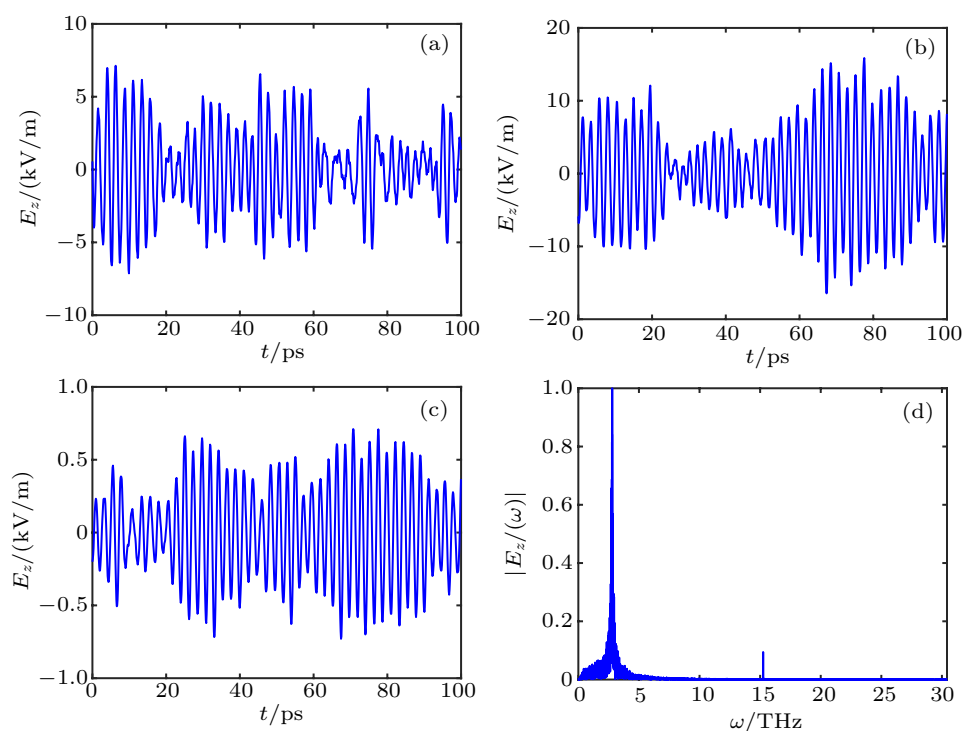


Fig. 4. Time-domain waveforms and frequency spectrum of high-frequency electromagnetic fields at points A, B, and C in Fig. 2.

The time-domain waveform and frequency spectrum characteristics of the high-frequency signal are introduced below. The time-domain characteristics of the electromagnetic field can be obtained by doing inverse Fourier transform of $\Delta A_\lambda(k, \omega)$ in Eq. (6). The time-domain waveform of the high-frequency electromagnetic field at $t = 5.0$ ms is shown in Figs. 4(a)–4(c) (The figure shows the high frequency oscillation within 100 ps). Figure 4(a) shows the time-domain waveform of the high-frequency electromagnetic field at $j = 30$ Ranvier’s node (point A in Fig. 2), figure 4(b) shows the time-domain waveform of the high-frequency electromagnetic field at $j = 31$ Ranvier’s node (point C in Fig. 2), and figure 4(c) shows the electromagnetic field at the midpoint of the 30th Ranvier’s node and the 31th Ranvier’s node (point B in Fig. 2). Figure 4(d) shows the frequency spectral characteristics of the time-domain waveform of the electromagnetic field in Fig. 4(a) (has been normalized).

In addition, the amplitude of the high-frequency electromagnetic field is stronger at Ranvier’s nodes, and the amplitude is weaker between Ranvier’s nodes. We believe that Ranvier’s node has an amplifying effect on high-frequency electromagnetic fields. The reason may be that there are ion channels at Ranvier’s node (the number of ion channels is very small at a location far away from Ranvier’s node), and the high-frequency ion transport current across the membrane at this location will excite high-frequency electromagnetic fields.

3.1. The effect of myelin length on signal transmission

The conduction of nerve signals between two adjacent Ranvier’s nodes is accomplished via “jumping conduction” in which the signal jumps from one Ranvier’s node to another, and the conduction speed is higher than that of unmyelinated neuron. Myelinated signals can be transmitted rapidly from several m/s up to more than 100 m/s.^[27] For the same nerve size, the conduction velocity of the unmyelinated nerve is slower than that of myelinated nerve fibres.

The appearance of the myelin structure significantly increases the conduction velocity of the nerve. Thus, is the myelin length as long as possible? The effect of the myelin length on nerve signal transmission is studied below. At the limit of myelin length $L \rightarrow +\infty$, the ion transmembrane transport current is $J_m = 0$. The eigenmode of the system dynamics equation is the attenuation of the travelling wave $e^{-\gamma t} e^{i(kx - \omega t)}$, which indicates that the length of the myelin sheath should have an upper limit or the signal amplitude will eventually return to zero, the numerical calculation results also confirm the above views. Assume that the myelin sheath is $L = 50$ cm (the length of the myelin sheath cannot be infinite in the actual calculation) and that the stimulation is applied at $x = 0$. Figure 5 shows the voltage signals at distances of 2.5 mm, 5.0 mm, and 7.5 mm from the stimulation posi-

tions, the signal amplitude of the time domain waveform decays rapidly.

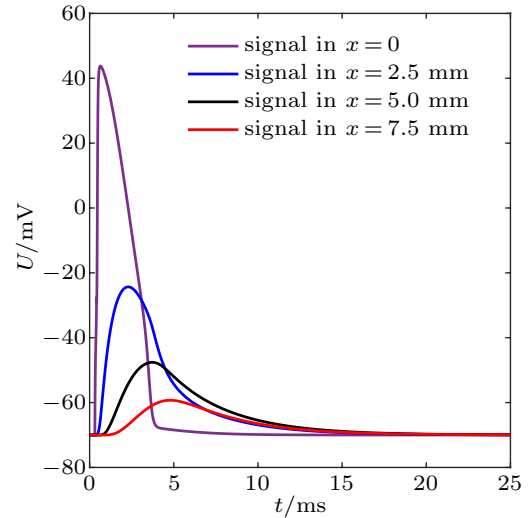


Fig. 5. Waveform of signals at different positions for myelin lengths $L \rightarrow +\infty$.

Since the length of the myelin sheath cannot be infinitely, in order to ensure that the signal can be transmitted along the nerve, what should be its maximum length? In this article, the problem is studied by changing the length of myelin sheath, the signal in A, B, and C (A, B, C are shown in Fig. 2) are recorded separately. As shown in Fig. 6. When the length of the myelin sheath is below a certain threshold l_T , the signal amplitude will remain unchanged when the signal is transmitted between two adjacent Ranvier’s nodes (Figs. 6(a) and 6(b)), once the length of the myelin sheath exceeds a certain threshold l_T , the neural signal cannot be effectively transmitted (Figs. 6(c) and 6(d)). (Note: Let V_k be the peak-to-peak value of the k -th Ranvier’s node membrane potential, due to the numerical error, V_{k+1} and V_k cannot be completely equal. In the calculation, while $V_{k+1}/V_k > 0.99$, the signal amplitude is regarded as almost unchanged, while $V_{k+1}/V_k < 0.99$, the signal can no longer be effectively transmitted). The value of l_T in different temperatures and neuron axon diameters is shown in Table 1 (Note: the calculation is accurate to 0.1 mm).

As shown in Table 1, to enable the signal to be transmitted in the range of 5 °C to 40 °C under the usual electrophysiological parameters, the length of the myelin sheath L cannot be larger than l_T ($T = 40$ °C), For myelinated nerves, the length L of the myelin sheath is proportional to the diameter d . Experimental results show that $L \approx 100d$.^[8] Whether it is $d = 5$ μm or $d = 10$ μm , both satisfy the condition $L < l_T$ ($T = 40$ °C), which is in good agreement with the above calculation results.

We give a preliminary explanation of the above calculation results. As shown in Fig. 5, the signal is attenuated in the absence of channel current. The above discussion believes that the signal energy will be supplemented when it passes through the Ranvier node, as the signal will adjust the switch of the ion

channel near the Ranvier node when it passes near the Ranvier node, generating a transmembrane ion transport current, which can be equivalent to a “current source” and play the role of energy supply. If the length of the myelin sheath is too long,

when the signal reaches the next Ranvier node from present Ranvier node, if its amplitude is already below the threshold of the excitation action potential, the action potential cannot be excited.

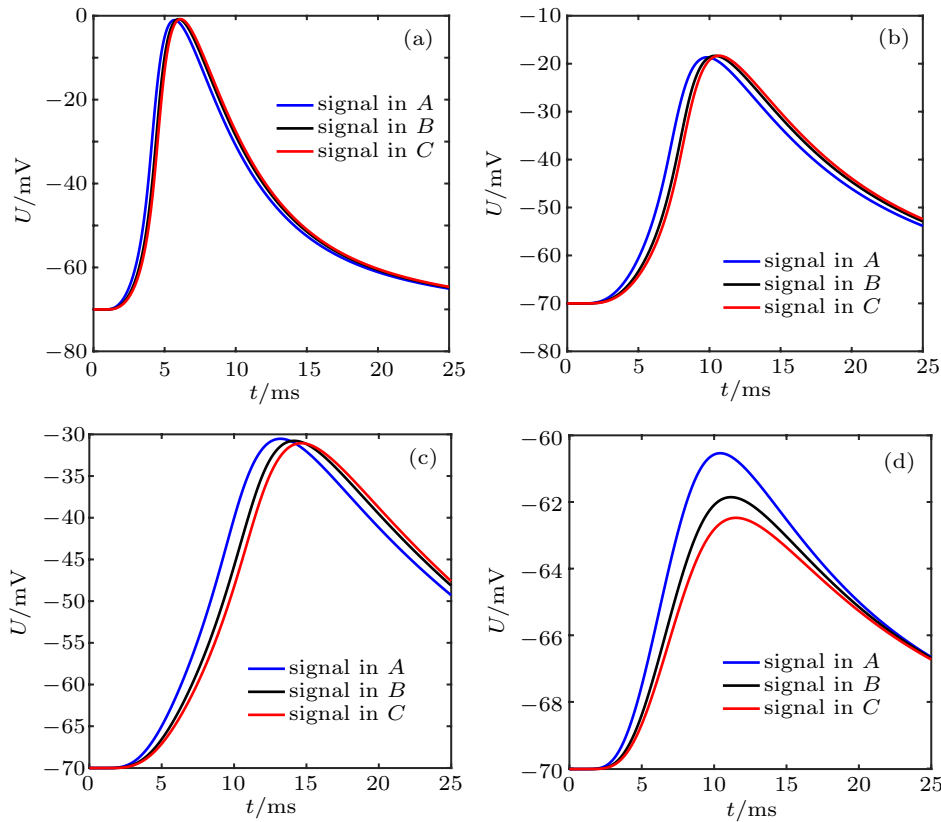


Fig. 6. The waveform of the action potential between two adjacent Ranvier’s nodes when the length of the myelin sheath is finite (panels (a)–(d) indicate that the length of the myelin sheath is 3 mm, 7 mm, 8.3 mm, and 10 mm, respectively, other parameters are set as follows: neuron diameter 5 μm , ambient temperature 10 $^{\circ}\text{C}$).

Table 1. Myelin length thresholds that guarantee signal recovery at different temperatures.

Temperature/ $^{\circ}\text{C}$	5	10	15	20	25	30	35	40
l_T/mm ($d = 5 \mu\text{m}$)	17.8	8.3	5.7	3.7	2.5	1.6	1.0	0.7
l_T/mm ($d = 10 \mu\text{m}$)	28.4	19.5	13.1	10.5	6.9	3.7	2.3	1.4

Based on the above discussion, the threshold length l_T of the myelin sheath depends on the nature of the ion current within the ion channel in Ranvier’s node. It is foreseeable that the density of ion channels also has an effect on signal transmission. The effect of different ion channel densities on signal transmission is studied below. The ion current is proportional to the density of the ion channel. Consider the threshold length l_T of the myelin sheath under the following two conditions: i) The density of potassium ion channels remains unchanged, and the density of sodium ion channels increases/decreases by 50% and 20%, respectively (this is reflected in the increase/decrease of sodium ion current respectively 50%, 20%); ii) The density of the sodium ion channel remains unchanged, and the density of the potassium ion channel increases/decreases by 50% and 20%, respectively (reflected in the increase/decrease of potassium ion current by

50%, 20%, respectively). The calculation results of the limit length of myelin sheath in different situations are shown in Fig. 7.

In Fig. 7, as the sodium channel density increases, the threshold length l_T of the myelin sheath also increases. Within the range of the selected calculation parameters, the threshold length l_T of the myelin sheath and the sodium ion channel density are approximately linear. The sodium ion channel density has a great influence on the signal transmission. For example, when the temperature is 15 $^{\circ}\text{C}$, the sodium ion channel density increases/decreases by 50%, and the myelin sheath’s threshold length l_T increases/decreases by about 60%. Contrary to sodium ion channels, within the range of selected calculation parameters, as the density of potassium ion channels increases, the threshold length l_T of myelin sheath decreases (the change in threshold length l_T of the myelin is very small). At 15 $^{\circ}\text{C}$,

the potassium channel density increases/decreases by 50%, and the myelin sheath's threshold length l_T changes by about 2%. According to the mechanism of the action potential generation, the sodium ion channel current excites the action potential through the depolarization current, while the potassium ion channel current restores the potential to the membrane potential level through polarization, increasing the sodium channel density can enhance depolarization and reduce the threshold of action potential. For potassium channels, the situation is just the opposite.

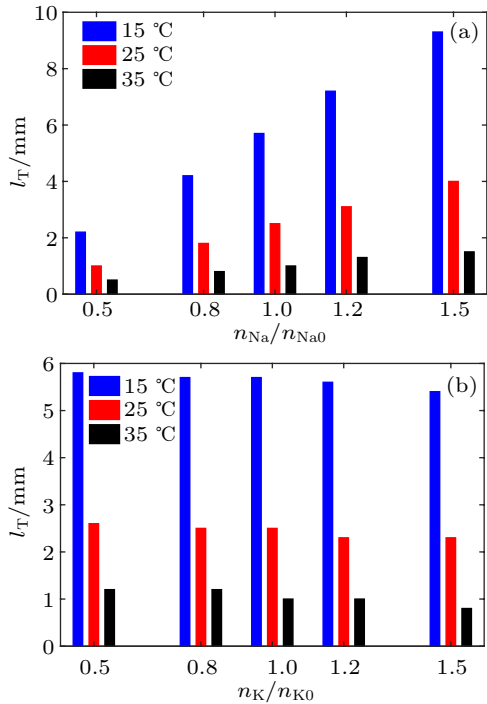


Fig. 7. The effect of ion channel density on the limit length of myelin sheath. Panel (a) indicates the effect of sodium ion channels and panel (b) indicates the effect of potassium ion channels (the neuron diameter is set to 5 μm).

3.2. The effect of temperature on signal of myelinated nerves

From the perspective of actual life experience, temperature will have a greater impact on the transmission of neural signals. Temperature mainly affects the transmission of electromagnetic field signals indirectly by affecting the medium characteristics of neurons. For example, temperature can affect the probability of ion channel switching, the interaction coupling coefficient between water molecules and electromagnetic field, ion–molecule scattering frequency, *etc.*, the influence of temperature on these parameters is shown in the [Supplementary file](#).

At first, we discuss the effect of temperature on nerve conduction velocity and action potential amplitude. the temperature sweep range is from 5 °C to 40 °C. The neuron diameter is set by 5 μm , 8 μm , 11 μm , 14 μm , 17 μm , and 20 μm .

The conduction velocity and voltage amplitude of the neural signal at different temperatures are shown in Fig. 8. The figure shows the following results: As the temperature

increases, the amplitude of the voltage signal decreases. Temperature influences the conduction velocity of low-frequency signals. The conduction velocity is the largest at a certain temperature T^* . When $T < T^*$, the conduction velocity increases with the temperature. When $T > T^*$, the conduction speed decreases with the temperature: For nerves with different diameters, the temperature T^* which the conduction velocity obtain its maximum does not differ significantly and is approximately $T^* = 306 \text{ K} = 33 \text{ }^\circ\text{C}$.

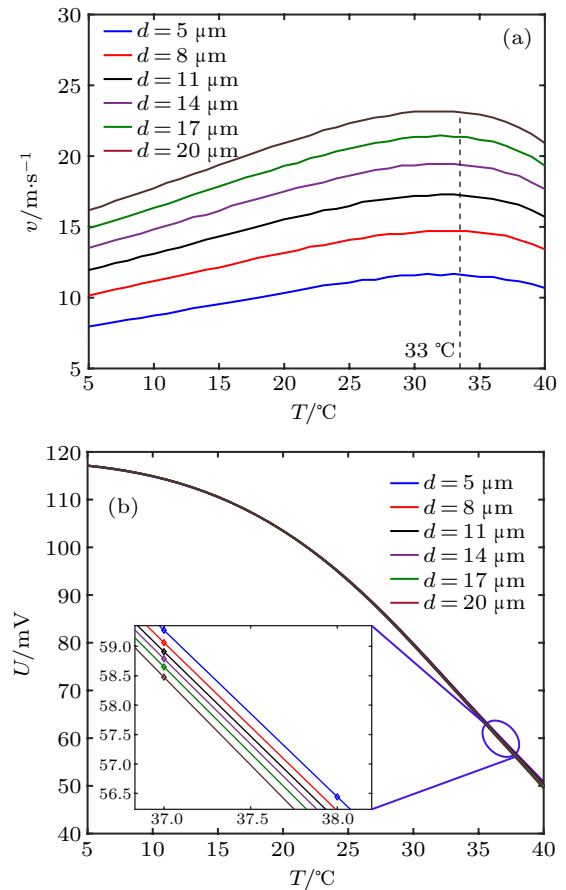


Fig. 8. Changes in the nerve conduction velocity (a) and membrane voltage (b) over time at different temperatures.

Figure 9 shows an experimental device used to measure the conduction velocity of the frog sciatic nerve at different temperatures. The standard physiological solution is prepared first, and then the physiological solution is placed at different temperatures using a temperature regulating device. The nerve is immersed in a physiological solution. After a sufficient thermal balance is reached, the conduction velocity of the nerve is measured.

Figure 10 shows the measurement results of the sciatic nerve conduction velocity of bullfrogs at different temperatures. Figures 10(a) and 10(b) show the measurement results when the temperature rises monotonously, figure 10(c) shows the measurement results when the temperature changes randomly, and figure 10(d) shows the measurement results when the temperature decreases monotonically.

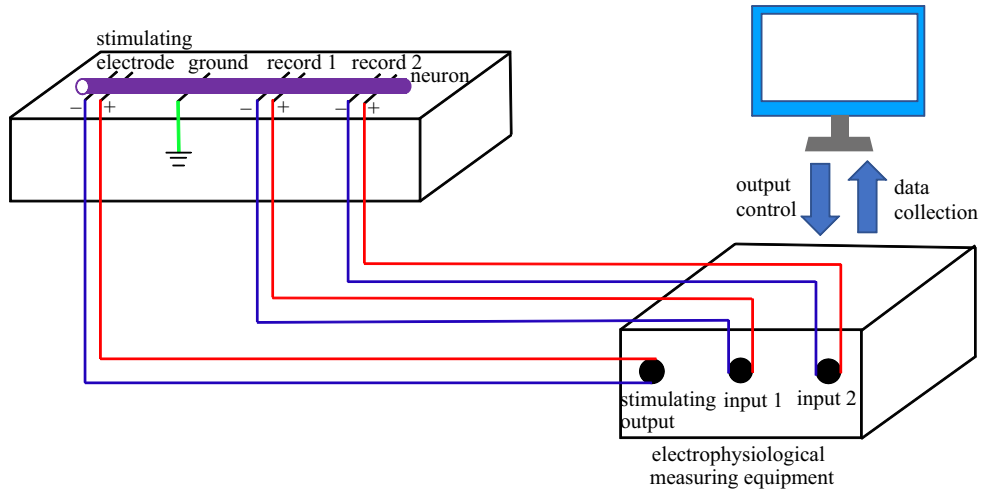


Fig. 9. The schematic diagram of frog sciatic nerve conduction velocity measuring device.

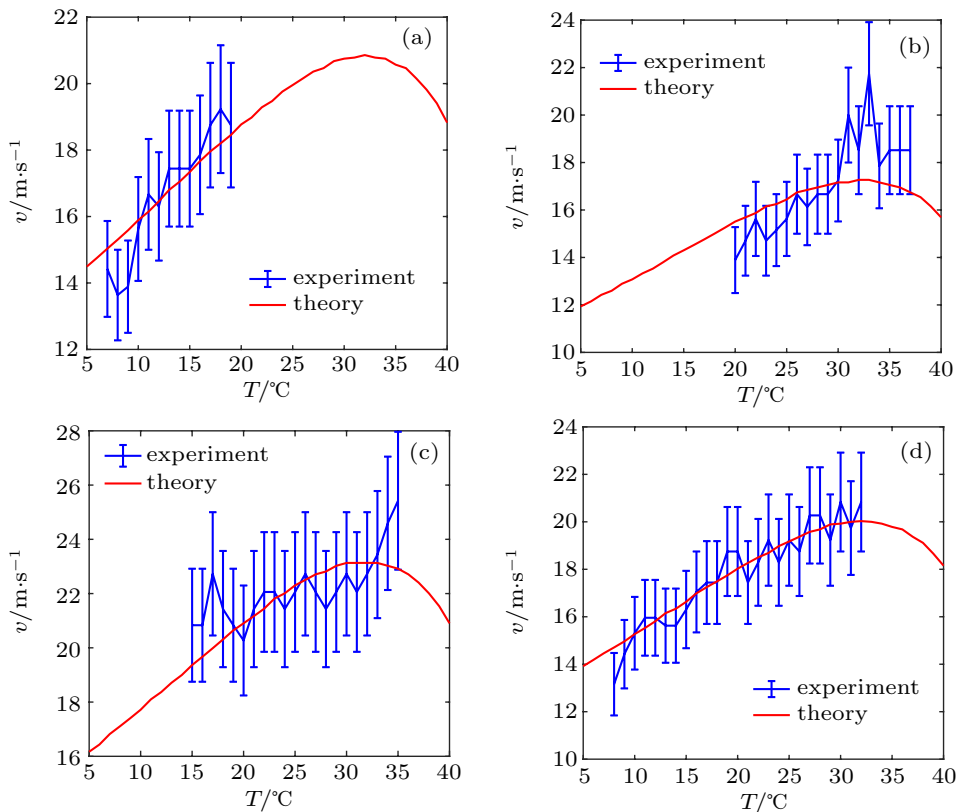


Fig. 10. Measurement of the nerve conduction velocity in a bullfrog at different temperatures. The red curve is the theoretical calculation result. Panels (a) and (b) show a monotonic rise in temperature. At the time of measurement, panel (c) shows a random temperature change (30 °C → 18 °C → 11 °C → 16 °C → 19 °C → 15 °C → 17 °C → 35 °C → 29 °C → 25 °C → 27 °C → 20 °C → 24 °C → 32 °C → 33 °C → 21 °C → 22 °C → 26 °C → 23 °C → 28 °C → 31 °C → 34 °C). Panel (d) shows the measurement results when the temperature decreases monotonically.

We compare the experimental data with the theoretical curve, considering that the conduction velocity is also related to the diameter of the neuron, note that the function of the conduction velocity change with temperature T and diameter d is $v(T, d)$, the experimental value at temperature T is $v_e(T)$, and define $f(d) = \sum_i |v(T_i, d) - v_e(T_i)|$ is the error between the theoretical value and the experimental value, the value of $d = d^*$ corresponding to the minimum value of the function $f(d)$ is calculated, and $v(T, d^*)$ is used as the theoretical curve. The values of d^* in Figs. 10(a)–10(d) are 16.1 μm ,

11.93 μm , 19.97 μm , and 14.87 μm , respectively.

Figure 10 shows that when the ambient temperature is lower than 32 °C, the nerve conduction velocity generally increases with increasing temperature. The theoretical curve and the experimental results are in good agreement (at certain temperature values, the experimental value and the theoretical value deviate), when the ambient temperature is higher than 32 °C, due to the limited measurement data and experimental errors, the relationship between temperature and conduction velocity still needs further study.

The effect of temperature on the transmission of high-frequency signals is discussed below. At 5 °C and 25 °C, the shock response spectrum of the system (*i.e.* $J(k, \omega) = 1$) is shown in Fig. 11 (the spectrum data in the figure have been normalized), the signal has two characteristic frequencies, which are denoted as mode 1 (lower frequency) and mode 2 (higher frequency).

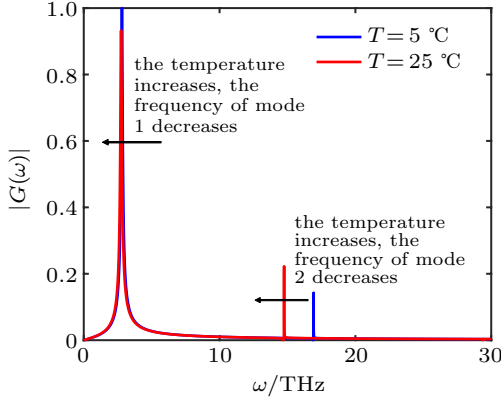


Fig. 11. The schematic diagram of effect of temperature on the signal spectrum, the signal has two characteristic frequencies, which are denoted as mode 1 (lower frequency) and mode 2 (higher frequency).

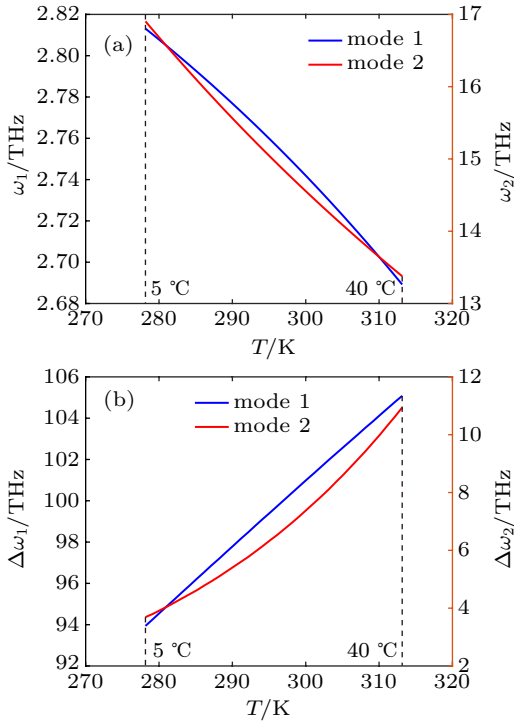


Fig. 12. The effect of temperature on the eigenmode, panel (a) represents the center frequency of the two modes, and panel (b) represents the bandwidth of the two modes, the modes 1 and 2 are represented by blue and red curves, respectively.

The frequency and bandwidth changes of the two eigenmodes with temperature are shown in Fig. 12. The following results were obtained.

1) The centre frequencies of both resonant modes decrease with increasing temperature (also shown in Fig. 11). The frequencies of modes 1 and 2 are

$$\omega_1 \approx \sqrt{(1 - 1/g^2)} \omega_p^2$$

and $\omega_2 \approx g\omega_0$,^[22] respectively. When the temperature increases, the water molecule distribution becomes more disordered. Then, the water molecule–field interaction coupling coefficient decreases, eventually leading to the centre frequency of the resonance mode, which decreases as the temperature increases.

2) The spectral widths of both resonance modes increase with increasing temperature because higher temperatures result in more irregular thermal motion of water molecules; additionally, the losses caused by system noise and irregular thermal motion change. The quality factor Q of the system decreases, and thus, the spectral widths of the two resonance modes increase.

Finally, we estimate the power of the signal and select a longer period of time Δt , then the average Energy density of the signal during this period can be calculated from

$$\langle W(\mathbf{r}) \rangle = \frac{1}{\Delta t} \int_0^{\Delta t} E^2(\mathbf{r}, t) + B^2(\mathbf{r}, t) dt$$

(using the natural unit), set the signal transmission speed to v (the velocity of the envelope), then the radiation power along the nerve conduction direction will be determined by

$$P = \int_R^{R+d} W(\mathbf{r}) v \cdot 2\pi r dr,$$

showing the electromagnetic field is mainly concentrated on the area where the water molecules formed ordered structures on the neuron surface (*i.e.*, $r \in (R, R+d)$) of the neuron, and the electromagnetic field outside this area is 0. The calculation result is shown in Fig. 13.

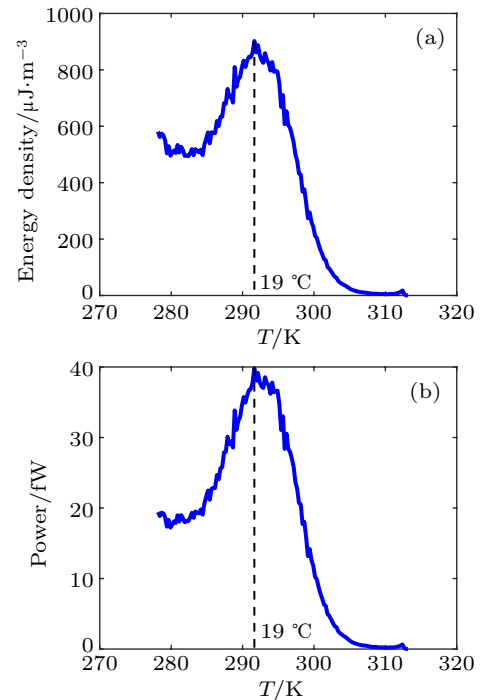


Fig. 13. The effect of temperature on the average electromagnetic field energy density at point A in Fig. 2(a) and the signal power (b) (the neuron diameter is 10 μm).

The calculation in Fig. 13 shows that at room temperature, the energy density of the high-frequency electromagnetic field signal is about hundreds of $\mu\text{J}/\text{m}^3$, and its power is about tens of fW. When the ambient temperature is about 19 °C, the energy density of the high-frequency electromagnetic field and the power both reach their maximum values.

4. Summary and discussion

This paper investigates the transmission of neural signals from myelinated neurons. The study found the following results.

(I) Compared with that of an unmyelinated nerve of the same size, the conduction velocity of a myelinated nerve is greatly increased. The appearance of the myelin sheath effectively reduces energy consumption. When transmitting on an unmyelinated nerve, energy must be replenished at any time, whereas when transporting along a myelinated nerve, energy only needs to be replenished at the Ranvier's node, which greatly improves the signal transmission efficiency.

(II) The length of the myelin sheath cannot be infinitely long. We found that within the range of suitable physiological parameters, when the length of the myelinated myelin sheath was less than a certain threshold l_T , the signal was attenuated when transmitted on the myelin sheath; additionally, signal amplitude occurred at the Ranvier's node. When the length of the myelin sheath exceeded l_T , the signal continued to decay and would not recover at the Ranvier's node. In the range of normal physiological parameters, l_T is in the order of mm.

(III) Both high and low temperatures are not conducive to transmission of nerve signals.

In this model, information is transmitted in the form of electromagnetic fields, the intrinsic frequency of the electromagnetic field signal transmitted along the nerve is in the order of THz, and the ion current formed by the ion transmembrane transport process will play a role in exciting the nerve high-frequency signal.

Some improvements could still be made in this paper. Firstly, the conclusions of the model are only theoretical predictions, and subsequent research needs to be verified by experiment. In addition, the theoretical model could also be improved as follows:

1) The numerical simulation study of ion transmembrane transport is rough, the motion of ions is simplified to one dimension, and the ion-ion channel interaction potential energy function is used.

2) The change in the ion channel switching probability with temperature is based on the curve obtained by experimental fitting. For the actual situation, the influence of temperature on the switching probability of ion channels is not explained in the physical mechanism.

3) The Lagrangian function of the system can be further improved. For example, considering the collective vibration mode of water molecules and small rotation around the equilibrium position, we can also consider the influence of multiple vibrational levels on water molecules.

4) This paper adopts the truncated boundary condition. In reality, the electromagnetic field outside the area where water molecules are ordered on the neuron surface is not completely zero. The actual calculation should be strictly solved using the medium parameters and boundary conditions of the region.

5) Only the intra- and extra-body material exchange process (achieved by the ion transmembrane transport process) is considered, and the energy coupling (electromagnetic interaction process) process inside and outside of the nerve is neglected. The deficiencies in these models will be further refined in future work.

Acknowledgments

The author thanks Professor Guo Guozhen, Professor Li Jing, Professor Xu Shenglong, Dr. Mao Honghui, Dr. Shang Mengjuan and Dr. Guo Zhouyang of The Fourth Military Medical University for their help in the experiment. The data that support the findings of this study are available from the corresponding author upon reasonable request.

References

- [1] Hodgkin A L and Huxley A F 1952 *The Journal of Physiology* **117** 500
- [2] Hodgkin A L and Huxley A F 1952 *The Journal of Physiology* **116** 449
- [3] Hodgkin A L and Huxley A F 1952 *The Journal of Physiology* **116** 497
- [4] Hodgkin A L, Huxley A F and Katz B 1952 *The Journal of Physiology* **116** 424
- [5] Hodgkin A L 1951 *Biol. Rev.* **26** 339
- [6] Hodgkin A L and Huxley A F 1952 *The Journal of Physiology* **116** 473
- [7] Izhikevich E M 2007 *Dynamical Systems in Neuroscience: The Geometry of Excitability and Bursting* (Massachusetts: MIT Press) pp. 31–50
- [8] Fitzhugh R 1962 *Biophys. J.* **2** 11
- [9] Goldman L and Albus J S 1968 *Biophys. J.* **8** 596
- [10] Moore J W, Joyner R W, Brill M H, Waxman S D and Najarjoa M 1978 *Biophys. J.* **21** 147
- [11] Tang R D and Dai J P 2014 *PLoS One* **9** 1
- [12] Devyatkov N D 1974 *Sov. Phys. Usp.* **16** 168
- [13] Traill R R 2011 *9th International Fröhlich's Symposium: Electrodynamic Activity of Living Cells (Including Microtubule Coherent Modes and Cancer Cell Physics)*, July 1–3, 2011, Prague, Czech Republic, p. 184
- [14] Kumar S, Boone K, Tuszynski J, Barclay P E and Simon C 2016 *Sci. Rep.* **6** 36508
- [15] Zangari A, Micheli D, Galeazzi R and Tozzi A 2018 *Sci. Rep.* **8** 539
- [16] Hameroff S R and Penrose R 2014 *Phys. Life. Rev.* **11** 94
- [17] Hameroff S and Penrose R 2014 *Phys. Life. Rev.* **11** 39
- [18] Hameroff S R, Craddock T J A and Tuszynski J A 2014 *J. Integr. Neurosci.* **13** 229
- [19] Hameroff S R and Watt R C 1982 *J. Theor. Biol.* **98** 549
- [20] Zhang X Q and Jiang L 2019 *Nano Research* **12** 1219
- [21] Liu G Z 2018 *Chin. Sci. Bull.* **63** 3864
- [22] Xiang Z X, Tang C X, Chang C and Liu G Z 2020 *Sci. Bull.* **65** 308
- [23] Xiang Z X, Tang C X, Chang C and Liu G Z 2020 *A new viewpoint and model of neural signal generation and transmission: signal transmission on unmyelinated neurons* (accepted in Nano Research)
- [24] Carstensen E L 1954 *J. Acoust. Soc. Am.* **26** 858
- [25] Ford M C, Alexandrova O, Cossell L, Stangemarten A, Sinclair J L, Koppescheinflug C, Pecka M, Attwell D and Grothe B 2015 *Nat. Commun.* **6** 8073
- [26] McNeal D R 1976 *IEEE Trans. Biomed. Eng.* **23** 329
- [27] Nicholls J G, Martin A R, Fuchs P A, et al. *From neuron to brain* (Sunderland, Massachusetts: Sinauer Associates) p. 135